Bi-modal Non-rigid Registration of Brain MRI Data Based on Deconvolution of Joint Statistics

David Pilutti, Maddalena Strumia, and Stathis Hadjidemetriou

University Medical Center Freiburg, 79106 Freiburg, Germany
david.pilutti@uniklinik-freiburg.de

Abstract. Images of different contrasts in MRI can contain complementary information and can highlight different tissue types. Such datasets often need to be co-registered for any further processing. A novel and effective non-rigid registration method based on the restoration of the joint statistics of pairs of such images is proposed. The registration is performed with the deconvolution of the joint statistics and then with the enforcement of the deconvolved statistics back to the spatial domain to form a preliminary registration. The spatial transformation is also regularized with Gaussian spatial smoothing. The registration method has been compared to B-Splines and validated with a simulated Shepp-Logan phantom, with the BrainWeb phantom, and with real datasets. Improved results have been obtained for both accuracy as well as efficiency.

Keywords: Non-rigid registration, joint statistics restoration, brain registration, multi-contrast registration.

1 Introduction

In brain imaging different MRI contrasts can provide complementary information for tissue properties. The resulting images often need to be co-registered for any further analysis. The registration can be intra-subject or inter-subject and can also be achieved effectively with a non-rigid representation.

To address this problem B-Splines methods have been widely used [8]. They represent misregistration with splines centered on grid node pixels. To make this method robust even in the case of contrast change, it has been combined with a distance measure such as the mutual information [9]. An alternative and commonly used registration method has been the Demons method [11]. It is based on a variational formulation and assumes constancy in image contrast. The Demons method has been combined with the normalized mutual information and has been applied to the registration of multi-modal brain MRI [6].

Mutual information is an extensively used distance measure for multi-modal registration [7, 12]. However the mutual information is a scalar quantity that under-constrains the registration. This contributes to making the methods using it computationally intensive particularly for volumetric datasets. In practice such methods must be combined with considerable spatial subsampling and/or multiresolution [4–6, 8, 9].

L. Shen et al. (Eds.): MBIA 2013, LNCS 8159, pp. 40–50, 2013.

The approach presented in this work is shown to be able to register brain images of different as well as similar MRI contrasts. The spatial misregistration is represented in terms of its effect on the joint statistics. It is assumed that the misregistration smooths the joint statistics. We propose a novel systematic non-rigid registration method that is based on the restoration of the joint statistics. The problem is approached as a statistical restoration, where the effect of the misregistration is represented as a convolution of the statistics with a Gaussian filter. The statistics are restored with a Wiener filter [13] that is used adaptively. The deconvolved statistics are enforced to the registration between the images to obtain an initial spatial transformation. Then, the transformation is regularized for smoothness.

The implementation of the proposed method is iterative and interleaves between the two constraints. The method has been compared with the Slicer3D implementation of the B-Splines registration. They have been compared over a variable contrast extension of the 3D Shepp-Logan simulated phantom [10], a modified BrainWeb phantom [1], and on several real datasets. It has been performed in full image resolution with significantly reduced computational requirements. The proposed method improves performance in terms of spatial resolution, computational efficiency, as well as accuracy.

2 Method

The misregistration between images distorts their joint statistics. In this work the distortion is considered as Gaussian smoothing of the joint statistics, which is deconvolved with adaptive Wiener filtering. This assumes a smoothness of anatomy in space and a larger size for anatomic structures compared to that of the extent of the misregistration. Misregistration is also assumed to be spatially smooth. As a pre-processing step, the two images are normalized in terms of resolution if necessary as well as in terms of their dynamic range. The method then performs an additional pre-processing step concatenating a rigid and an affine registration. The result is then used to initialize the subsequent non-rigid registration.

The problem of the non-rigid registration of pairs of images is formulated with two priors. The first results from the deconvolution of the joint intensity statistics with the adaptive Wiener filter. The second results from the spatial regularization of the registration with a Gaussian filter. The method interleaves between the two priors iteratively, $k = 0, ..., K-1$ for a total of K iterations. An overview of the registration is given with the diagram shown in Fig. 1. A pairwise registration is between a reference image I_{ref} and a moving image I_{mov}. A spatial transformation $\mathbf{T} = (u_x, u_y, u_z)$ from I_{ref} to I_{mov} is estimated to obtain the registered image $I_{reg} = I_{mov}(\mathbf{T}^{-1}(\mathbf{x}))$ where $\mathbf{x} = (x, y, z)$ are the spatial coordinates. The registration can accommodate a variable contrast. The method allows the registration over a limited Region Of Interest (ROI) over the image for which the contrast is intended for and is meaningful.

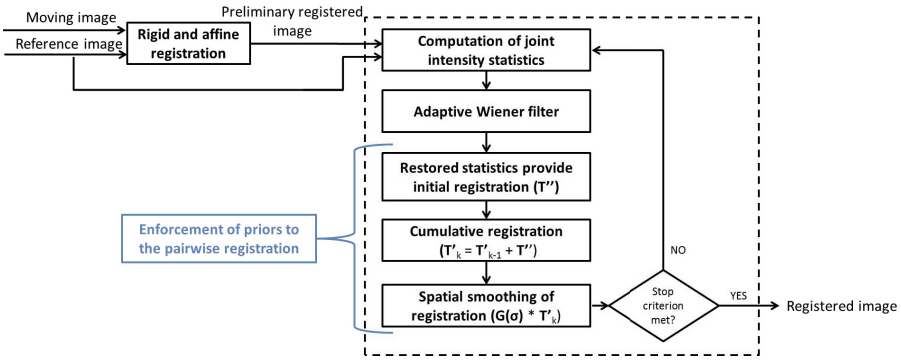

Fig. 1. Diagram describing the registration of two images with the proposed registration method. A preliminary rigid and affine registration is performed and the result is used to initialize the iterative non-rigid registration step until the stop criterion is met.

2.1 Computation of the Joint Intensity Statistics and Their Wiener Restoration

Two images I_{ref} and I_{mov} under assumed perfect alignment give rise to the joint histogram H_{ideal}. The joint statistics H_0 of the misregistered images are considered to result from the convolution of H_{ideal} with a 2D Gaussian filter $G_{Hi,j}(\sigma_H)$:

$$H_0 = H_{ideal} * G_{Hi,j}(\sigma_H) + n_H, \tag{1}$$

where σ_H is the standard deviation of the Gaussian convolution, $*$ is the convolution, n_H is the noise and i, j are the indices for the dynamic ranges of I_{ref} and I_{mov}, respectively. The statistics H_0 are deconvolved with a 2D adaptive Wiener filter

$$f_{i,j} = \frac{G_{Hi,j}}{||G_{Hi,j}||_2^2 + \epsilon}, \tag{2}$$

where ϵ assumes a small value. The filter $f_{i,j}$ is convolved with H_0 to obtain an estimate of the restored deconvolved statistics with:

$$H_{rest} = f_{i,j} * H_0. \tag{3}$$

Fig. 2 shows two images and their joint statistics at different iterations before the Wiener deconvolution. The deconvolved statistics are used as a prior to constrain the estimation of the registration.

2.2 Adaptive Wiener Filter

The distortion in the joint statistics is assumed to be non-stationary throughout the dynamic ranges, depending on properties of different tissues. This has been modeled with an adaptive Wiener filter to preserve the distributions corresponding to different tissue types. The focus has been given to the estimation

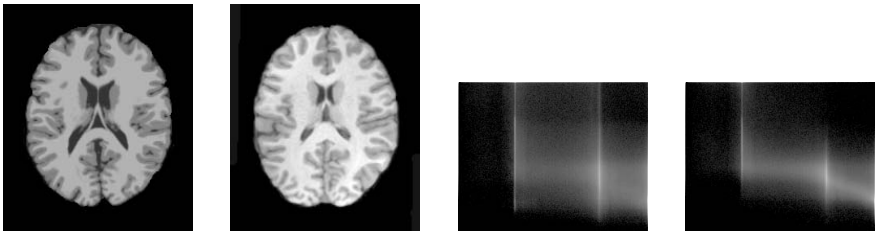

(a) Reference (b) Moving (c) Iteration 0 (d) Iteration 30

Fig. 2. Joint statistics for initial images (a) and (b) before Wiener deconvolution at the initial iteration (c) and after 30 iterations (d). The joint statistics in (d) become sharper.

of the local mean $\mu_{H_0}(i,j)$ and variance $\sigma^2_{H_0}(i,j)$ over a moving window of size $(2r+1) \times (2s+1)$. The local mean $\mu_{H_0}(i,j) = \langle H_0 \rangle_{r,s}$ and the local variance ${\sigma_{H_0}}^2(i,j) = \langle H_0^2 \rangle_{r,s} - \langle \mu_{H_0} \rangle^2_{r,s}$ are estimated over the observed joint statistics H_0 of the misregistered images. The standard deviation $\sigma_W(i,j) \propto \sqrt{\frac{1}{\sigma^2_{H_0}(i,j)}}$, where σ_W is the standard deviation of the Wiener filter, used to represent the local variance of the Gaussian distortion and in turn to appropriately adjust the Wiener filter. Thus, the Wiener filter width becomes smaller as the distributions become steeper and is able to preserve their sharpness.

2.3 Enforcement of Priors to the Pairwise Registration

The two considered images I_{ref} and I_{mov} are used to construct a graph $R = (V, E)$. Each voxel of the image corresponds to a vertex in V. The edges in E are connecting each node in I_{ref} to nodes in a 6-connected spatial neighborhood $\mathcal{N}$ in I_{mov}, $\mathcal{N}(\mathbf{x}) = \mathbf{x}+\Delta\mathbf{x}$, where $\Delta\mathbf{x} = (\pm\Delta x, \pm\Delta y, \pm\Delta z)$ and $\Delta x, \Delta y, \Delta z$ are the sizes of a voxel along the axes. The voxel anisotropy is accounted for by using an edge weight $w_d = 1/(d+1)$ for a distance d.

The intensities of the edge between $I_{ref}(\mathbf{x})$ and $I_{mov}(\mathbf{x}+\Delta\mathbf{x})$ form an index for the restored joint histogram H_{rest} to retrieve the second edge weight $w_H = H_{rest}(I_{ref}(\mathbf{x}), I_{mov}(\mathbf{x}+\Delta\mathbf{x}))$. The product $w_{tot}(\mathbf{x}, \Delta\mathbf{x})$, $w_{tot} = w_d \cdot w_H$ gives the total weight of an edge. The linear expectation of the direction of the edges connecting $\mathbf{x}$ over their weights gives an initial displacement $\mathbf{T}''(\mathbf{x})$ for voxel at $\mathbf{x}$. At iteration k the displacements over the entire image give an initial transformation

$$\mathbf{T}''_k(\mathbf{x}) = \mathbf{x} + E_{w_{tot}}(\mathbf{x}, \Delta\mathbf{x}) = \mathbf{x} + \frac{\Sigma_{\mathcal{N}} w_{tot}(\mathbf{x}, \Delta\mathbf{x})(\Delta\mathbf{x})}{\Sigma_{\mathcal{N}} w_{tot}(\mathbf{x}, \Delta\mathbf{x})}. \tag{4}$$

This is accumulated to obtain $\mathbf{T}'_k = \mathbf{T}'_{k-1} + \mathbf{T}''_k$. The second prior is the spatial regularization. To regularize the estimation of the transformation $\mathbf{T}'_k$, the gradient magnitude $||\nabla \mathbf{T}'_k||_2$ over the image is penalized, that is equivalent to the application of a 3D Gaussian filter $G(\mathbf{x}; \sigma_S)$ with standard deviation σ_S to the

spatial transformation $\mathbf{T}'_k$ at iteration k that gives the final estimate of the total transformation $\mathbf{T}_k = \mathbf{T}'_k * G(\mathbf{x}; \sigma_S)$.

2.4 Order of Computational Complexity

The complexity of the method developed in this work is significantly lower compared to that of the multicontrast extension of the B-Splines method with the mutual information for the same spatial resolution. In fact, the proposed method even when operating in full spatial resolution significantly expedites the non-rigid registration task compared to the B-Splines. The computational cost of the registration is expressed as a function of: K-number of iterations, m-effective size for each of the image dimensions, n-size of a neighborhood window $n = |\mathcal{N}|$ around a pixel, p-spatial subsampling factor between nodes, and σ_S of the regularizer. In the proposed method the pairwise registration requires the computation and deconvolution of the joint statistics as well as the spatial smoothing only once per iteration. This is in contrast to the B-Splines method extended with the MI that requires the joint statistics estimation and the spatial smoothing $|\mathcal{N}|$ times for each of the $(m/p)^3$ nodes in every iteration to cover the entire image. The complexity of our method is $O([m^3 n + m^3 3\sigma_S]K)$, while that of the B-Splines method with the MI is $O((m/p)^3 n[m^3 n + m^3 3\sigma_S]K)$.

The cost of the Demons method extended with the MI can be even higher than that of the B-Splines depending on the levels l of the multiresolution pyramids it is often combined with. Assuming that the image widths are halved at every level, the cost is $O\left(\left(\sum_{l'=0}^{l'=l-1}\left(\frac{m}{2^{l'}}\right)^3\right) n[m^3 n + m^3 3\sigma_S]K\right)$.

3 Experiments and Results

3.1 Implementation of Method and End Condition of Iterations

The method has been implemented in $C{+}{+}$. To improve performance the adaptive Wiener filter for the statistics has been implemented separably and is approximated as $f_{i,j} = \frac{G_{Hi}}{||G_{Hi}||_2^2+\epsilon} * \frac{G_{Hj}}{||G_{Hj}||_2^2+\epsilon}$ assuming that $G_{Hi,j} = G_{Hi} * G_{Hj}$, where G_{Hi} and G_{Hj} are 1D Gaussian filters. The value of the inverse signal to noise ratio ϵ for the adaptive Wiener filter has been set to 0.1. The spatial regularization $G(\mathbf{x}; \sigma_S)$ of the transformation has been performed using the ITK [2] implementation of the 3D recursive separable Gaussian filter along each of the components of the displacements u_x, u_y and u_z along the three axes. The pairwise non-rigid registration method developed is preceded by the rigid and affine registration methods provided by ITK [2]. The method processes 3D images.

The optimization iteratively alternates between the constraints arising from the statistical restoration and from the spatial regularization. The convergence of the registration is evaluated at every iteration. It uses the average L_2 norm of the spatial transformation $||T_k||$. The stop condition s of the iterations is $s = \frac{||T_k||}{||T_0||} - 1 < -1\%$. A maximum number of $s_{max} = 50$ iterations is also enforced.

3.2 Validation Methodology

To evaluate the quality of the registration obtained from phantom datasets with the method presented, the voxelwise Sum of Absolute Differences $SAD = ||I_{true}(\mathbf{x}) - I_{reg}(\mathbf{x})||_2$, where I_{true} is the true reference image in case of phantoms, has been calculated within a ROI between the true and the registered image. The percent improvement (Imp) of SAD is defined as $Imp_{SAD\%} = \frac{SAD_{bef} - SAD_{aft}}{SAD_{bef}} 100\%$, where SAD_{bef} and SAD_{aft} represent the SAD calculated before and after the registration, respectively. The registration of the bi-contrast real datasets has been evaluated by observation and by calculating the percent improvement in MI $Imp_{MI\%} = \frac{MI_{aft} - MI_{bef}}{MI_{aft}} 100\%$ before and after registration.

The method has been compared with the pairwise B-Splines based non-rigid registration method provided by Slicer3D [3]. The configuration of Slicer3D includes also a rigid and affine pre-registration steps as does the proposed method. MI has been used as a metric for all the registration steps. The tests were performed on a workstation with an Intel Core2 Duo 3.0 GHz CPU and 16GB of RAM. Our non-optimized implementation of the proposed method for a typical image can be further improved to achieve a high upper bound of speedup and had a 260% lower working memory requirement compared to the B-Splines method as shown in Table 1. It also operates in full image resolution as opposed to the B-Spline method that in practice requires subsampling. The B-Splines method tested operates in a grid of size $20 \times 20 \times 20$, which in the case of the BrainWeb phantom dataset gives a resolution of $9 \times 10.8 \times 9mm^3 = 875mm^3$ as subsampling. The presented method operates in full spatial resolution of $1 \times 1 \times 1mm^3 = 1mm^3$, which provides a resolution 875 times higher. The quantitative results and comparisons of the proposed method to those of the B-Splines method are shown in Table 1.

3.3 Shepp-Logan Phantom Data

A dataset for the validation of the proposed method has been a multicontrast simulation from the 3D Shepp-Logan phantom with a full resolution of $128 \times 128 \times 128$ pixels as displayed in Fig. 3 which shows an obvious improvement in alignment. The phantom has been modified to simulate the contrast change and a 3D sinusoidal function over the spatial image coordinates in all dimensions has been applied to simulate a non-rigid transformation. The value of σ_S for the spatial smoothing has been set to 6 voxels. The registration has been performed within a manually specified ROI shown in Fig. 3d. After 8 iterations it can be seen in Fig. 3 that the phantom is properly registered. The registration between I_{ref} and I_{mov} gives an $Imp_{SAD\%}$ of about 68%. A performance comparison with the B-Splines method is shown in row 1 of Table 1, where it is shown that the proposed method improves the accuracy.

3.4 BrainWeb Phantom Data

Another validation phantom data has been obtained from the BrainWeb database as shown in Fig. 4. The phantom data consists of two images with a full resolution

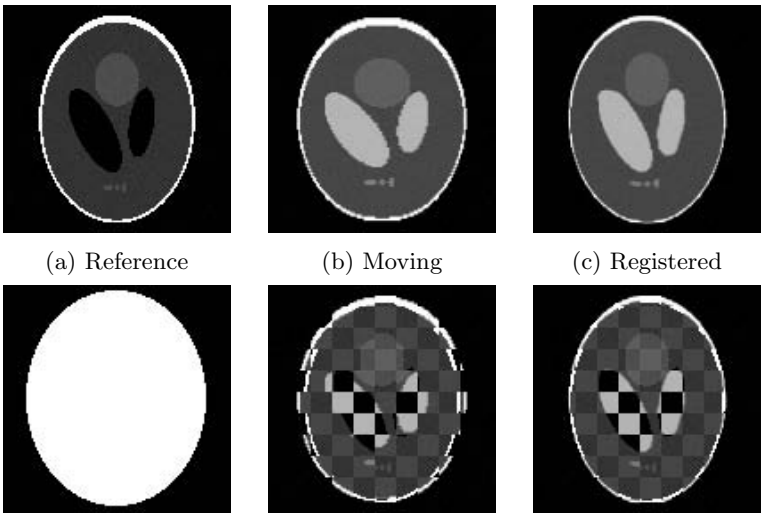

(a) Reference (b) Moving (c) Registered

(d) ROI mask (e) Before (f) After

Fig. 3. A 2D axial slice from the 3D Shepp-Logan phantom. (a) is the reference image, (b) is the misregistered image, (c) is the registered image obtained with the proposed method, and (d) is the ROI used. In (e) and (f) are the checkerboard compositions interleaving I_{ref} and I_{mov} before and after the registration.

of $180 \times 216 \times 180$ pixels taken using a T_1 and a T_2 sequences. The T_1 image has been used as reference. A non-linear misregistration has been simulated with a 3D sinusoid and has been applied to the T_2 image. The images were subsequently registered and the results are shown in the images in Fig. 4 and in row 2 of Table 1.

3.5 Real Brain Data

The real brain data in this study is composed of 5 young healthy volunteers. The study was approved by the local internal review board and the volunteers provided informed consent. The images were acquired with a 3T Siemens Trio MRI system equipped with head coils. The acquisition protocol consisted of a 3D T_1 and FLAIR sequences. The T_1 and FLAIR sequences give a matrix of size $512 \times 512 \times 160$ with a voxel of resolution $0.5 \times 0.5 \times 1mm^3$.

All real datasets were placed in the same anatomic space and the BrainWeb T_1 dataset has been chosen as the reference image. Fig. 5 shows an example of the registration between the T_1 BrainWeb phantom and a T_1 image from a volunteer. In Fig. 6 is an example of the registration between the T_1 BrainWeb phantom and a FLAIR image from a volunteer. The misregistered images shown in Fig. 5b and 6b are the results of the rigid and affine registration steps and are used as input for the non-rigid registration method proposed. The red arrows highlight the effect of the registration on significant brain structures.

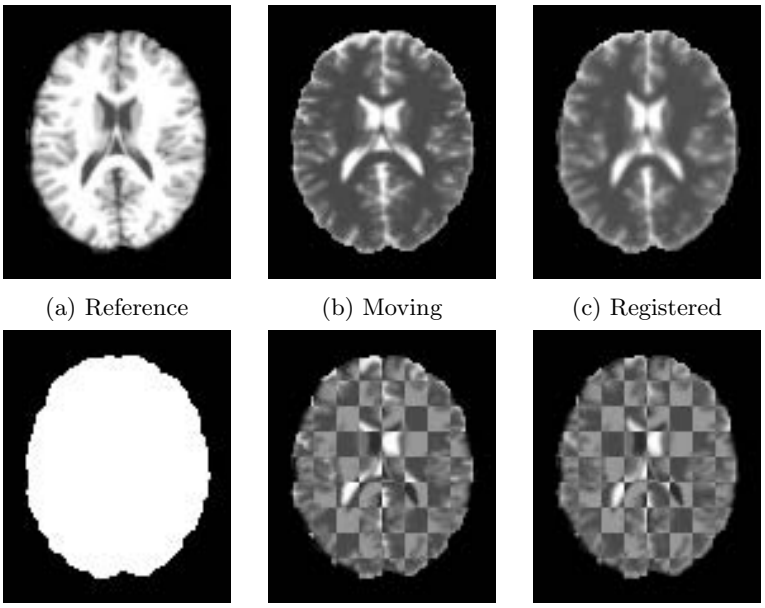

(a) Reference (b) Moving (c) Registered

(d) ROI mask (e) Before (f) After

Fig. 4. A 2D axial slice from the 3D BrainWeb phantom. (a) is the reference image, (b) is the misregistered image, and (c) is the registered image obtained with the proposed method. (d) is showing the ROI used, and (e) and (f) are the checkerboard compositions interleaving I_{ref} and I_{mov} before and after the registration.

Table 1. Performance and comparison of the proposed method with that of the Slicer3D optimized implementation of B-Splines

Datasets	Method	Imp (SAD%)	Imp (MI%)	Resol. (voxels)	Exec. time	Memory Space
Shepp-Logan Phantom	B-Splines	65.13%		1/262	∼1min	730MB
	Proposed	68.54%		1	∼18min	450MB
BrainWeb Phantom	B-Splines	47.39%		1/875	∼2min	4GB
	Proposed	64.11%		1	∼ 90min	2GB
Volunteer 1	B-Splines		52.06%	1/875	∼2min	4GB
	Proposed		57.35%	1	∼90min	2GB
Volunteer 2	B-Splines		29.30%	1/875	∼2min	4GB
	Proposed		32.31%	1	∼90min	2GB
Volunteer 3	B-Splines		44.65%	1/875	∼2min	4GB
	Proposed		58.39%	1	∼90min	2GB
Volunteer 4	B-Splines		38.54%	1/875	∼2min	4GB
	Proposed		56.13%	1	∼90min	2GB
Volunteer 5	B-Splines		19.28%	1/875	∼2min	4GB
	Proposed		31.93%	1	∼90min	2GB

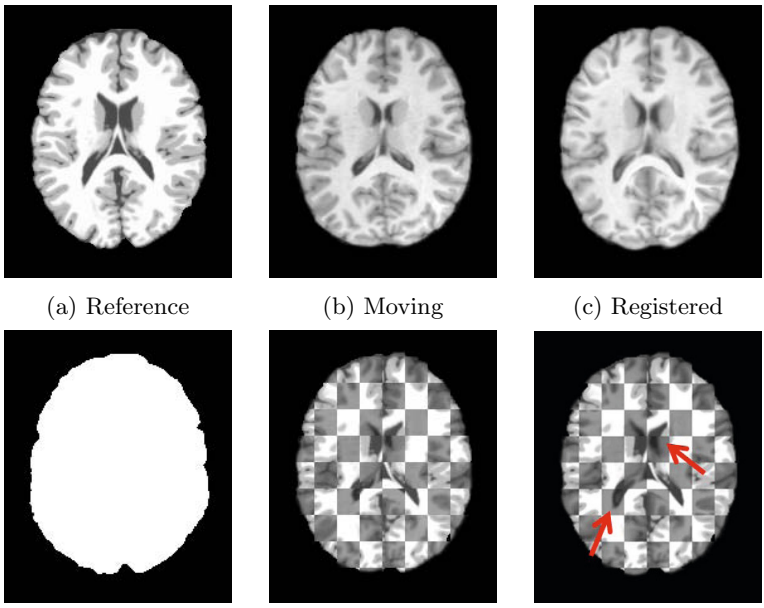

(a) Reference (b) Moving (c) Registered

(d) ROI mask (e) Before (f) After

Fig. 5. A 2D axial slice of a 3D real patient T_1 dataset registered to the T_1 BrainWeb phantom. (a) is the reference image, (b) is the misregistered image, (c) is the registered image obtained with the proposed method, and (d) is the ROI used. In (e) and (f) are the checkerboard compositions interleaving I_{ref} and I_{mov} before and after the registration. The red arrows highlight the effect of the registration on significant brain structures.

4 Summary and Discussion

Almost all the parameters of the method are held fixed for all the datasets. The only variable parameter is the σ_S of the spatial regularizer, which should be at most equal to the spatial variation of the displacement field. The parameter σ_W of the adaptive Wiener filter has been set with a proportionality constant so that its value is less than than of the width of the distributions of the tissues to preserve them. As shown analytically the order of computational complexity is lower than that of both the B-Splines and of the Demons method. The overall speedup is a power of the dimensionality of the considered datasets. The total time performance of the methods is shown in Table 1 and includes the common cost of the rigid and affine pre-processing steps. The relatively high time performance obtained by B-Splines in Slicer3D is due to the optimized software implementation and use of hardware such as multicore CPUs. However, it was not possible to test Slicer3D B-Splines with full resolution because of its excessive memory requirements.

The method developed significantly improves efficiency and accuracy of non-rigid registration of multi-modal brain datasets while operating at full spatial

resolution. The method shows an improvement qualitatively in terms of visual comparison as well as quantitatively in terms of $Imp_{SAD\%}$, and $Imp_{MI\%}$. The method is based on a systematic model of the misregistration and its removal. It has accurately compensated the misregistration in phantoms as well as in several multi-modal real brain datasets. The non-rigid registration can accommodate both same as well as different image contrasts. It is iterative and results in an effective deconvolution of the joint statistics that only requires a single estimation of the joint statistics and the spatial smoothing per iteration that covers the entire image. The registration method proposed does not involve the MI distance measure. The MI allows more degrees of freedom than necessary and can lead to a significantly higher computational cost. The performance of this method as well as of all methods based on image statistics is improved if an ROI of meaningful contrast is considered.

An advantage of the method proposed is that it is robust to the anisotropic resolution present in the clinical imaging data of this study. The method developed in this work performs a dense spatial registration robust against contrast changes and anisotropy. The presented method can be extended to 4D data for an even higher expected comparative upper bound in speedup.

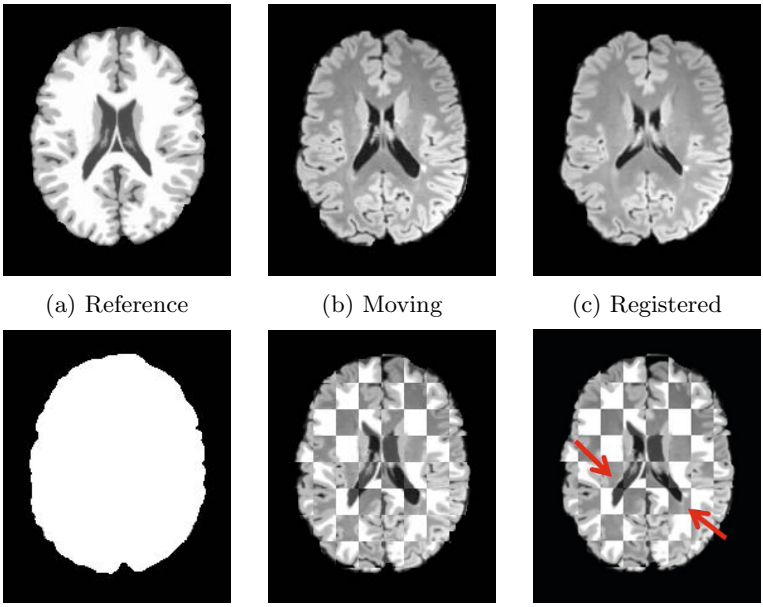

(a) Reference (b) Moving (c) Registered

(d) ROI mask (e) Before (f) After

Fig. 6. A 2D axial slice of a 3D real patient FLAIR dataset registered to the T_1 BrainWeb phantom. (a) is the reference image, (b) is the misregistered image, (c) is the registered image obtained with the proposed method, (d) is the ROI used. In (e) and (f) are the checkerboard compositions interleaving I_{ref} and I_{mov} before and after the registration. The red arrows highlight the effect of the registration on significant brain structures.

References

1. Collins, D.L., Zijdenbos, A.P., Kollokian, V., Sled, J.G., Kabani, N.J., Holmes, C.J., Evans, A.C.: Design and construction of a realistic digital brain phantom. IEEE Trans. on Medical Imaging 17(3), 463–468 (1998)
2. Ibanez, L., Schroeder, W., Ng, L., Cates, J.: The ITK Software Guide, 2nd edn. Kitware, Inc. (2005) ISBN 1-930934-15-7
3. Johnson, H., Harris, G., Williams, K.: Brainsfit: Mutual information registrations of whole-brain 3D images, using the Insight Toolkit. Insight J. (2007), `http://www.slicer.org`
4. Lu, H., Reyes, M., Serifovic, A., Weber, S., Sakurai, Y., Yamagata, H., Cattin, P.: Multi-modal diffeomorphic Demons registration based on point-wise mutual information. In: Proc. of IEEE ISBI, pp. 372–375. IEEE (2010)
5. Martel, A., Froh, M., Brock, K., Plewes, D., Barber, D.: Evaluating an optical-flow-based registration algorithm for contrast-enhanced magnetic resonance imaging of the breast. Physics in Medicine and Biology 52, 3803 (2007)
6. Modat, M., Vercauteren, T., Ridgway, G., Hawkes, D., Fox, N., Ourselin, S.: Diffeomorphic Demons using normalised mutual information, evaluation on multi-modal brain MR images. SPIE-The International Society for Optical Engineering (2010)
7. Pluim, J.P.W., Maintz, J.B.A., Viergever, M.A.: Mutual-information-based registration of medical images: a survey. IEEE Transactions on Medical Imaging 22(8), 986–1004 (2003)
8. Rueckert, D., Sonoda, L., Hayes, C., Hill, D., Leach, M., Hawkes, D.: Non-rigid registration using free-form deformations: application to breast MR images. IEEE Trans. on Medical Imaging 18(8), 712–721 (1999)
9. Rueckert, D., Aljabar, P., Heckemann, R.A., Hajnal, J.V., Hammers, A.: Diffeomorphic registration using B-splines. In: Larsen, R., Nielsen, M., Sporring, J. (eds.) MICCAI 2006. LNCS, vol. 4191, pp. 702–709. Springer, Heidelberg (2006)
10. Schabel, M.: 3D Shepp-Logan phantom. MATLAB Central File Exchange, pp. 1–35 (2006)
11. Thirion, J.: Image matching as a diffusion process: an analogy with Maxwell's Demons. Medical Image Analysis 2(3), 243–260 (1998)
12. Wells III, W., Viola, P., Atsumi, H., Nakajima, S., Kikinis, R.: Multi-modal volume registration by maximization of mutual information. Medical Image Analysis 1(1), 35–51 (1996)
13. Wiener, N.: Cybernetics: or the Control and Communication in the Animal and the Machine, vol. 25. MIT Press (1965)